JACS
JOURNAL OF THE AMERICAN CHEMICAL SOCIETY

Article

pubs.acs.org/JACS

Branchpoint Expansion in a Fully Complementary Three-Way DNA Junction

Tara Sabir,[†,‡] Anita Toulmin,[†,‡] Long Ma,[§] Anita C. Jones,[§] Peter McGlynn,[⊥] Gunnar F. Schröder,*[,∥] and Steven W. Magennis*[,†,‡]

[†]The School of Chemistry and [‡]The Photon Science Institute, Alan Turing Building, The University of Manchester, Oxford Road, Manchester M13 9PL, U.K.

[§]EaStCHEM School of Chemistry and Collaborative Optical Spectroscopy, Micromanipulation and Imaging Centre, The University of Edinburgh, West Mains Road, Edinburgh EH9 3JJ, U.K.

[⊥]Institute of Medical Sciences, University of Aberdeen, Ashgrove Road West, Aberdeen AB25 2ZD, U.K.

[∥]Institute of Complex Systems (ICS-6), Forschungszentrum Jülich, 52425 Jülich, Germany

Supporting Information

ABSTRACT: Branched nucleic acid molecules serve as key intermediates in DNA replication, recombination, and repair; architectural elements in RNA; and building blocks and functional components for nanoscience applications. Using a combination of high-resolution single-molecule FRET, time-resolved spectroscopy, and molecular modeling, we have probed the local and global structure of a DNA three-way junction (3WJ) in solution. We found that it adopts a Y-shaped, pyramidal structure, in which the bases adjacent to the branchpoint are unpaired, despite the full Watson−Crick complementarity of the molecule. The unpairing allows a nanoscale cavity to form at the junction center. Our structure accounts for earlier observations made of the structure, flexibility, and reactivity of 3WJs. We anticipate that these results will guide the development of new DNA-based supramolecular receptors and nanosystems.

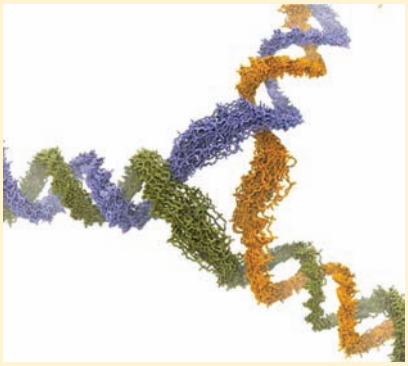

INTRODUCTION

Branched nucleic acid molecules are central intermediates in genome duplication, repair of DNA damage, and site-specific and homologous recombination between DNA duplexes, and are also important architectural elements in RNA.[1,2] Branched DNA and RNA are also widely used as building blocks in nanotechnology applications,[3−5] including nanomechanical devices,[6,7] macroscopic self-assembly,[8] molecular computation,[9] and DNA origami.[10] In spite of this, there are few high-resolution structural studies of DNA and RNA junctions, a notable exception being the four-way Holliday junction.[11]

An emerging quantitative structural tool, which is complementary to standard methods such as crystallography and NMR, is single-molecule Förster resonance energy transfer (SM-FRET).[12,13] SM-FRET probes inter- or intramolecular energy transfer between chromophoric labels on the 1−10 nm length scale,[14,15] making it ideal for studying the structure and dynamics of nucleic acid structures.[16] While it is well known that the distance dependence of FRET can be used as a molecular ruler, the determination of absolute distances requires knowledge of the relative orientations and mobility of the donor and acceptor dyes. We recently used a combination of multiparameter SM-FRET and molecular dynamics (MD) to produce a 3D global structure of a forked DNA molecule in solution, free of ensemble averaging.[17]

Here we have determined the 3D global structure of a fully complementary DNA three-way junction (3WJ) in solution using a combination of high-resolution SM-FRET, molecular dynamics, and time-resolved fluorescence of the nucleobase analogue 2-aminopurine (2-AP) to probe the local DNA structure.[18] Unlike the four-way DNA junction, 3WJs have received relatively little attention to date, though they are prevalent *in vivo* and in nanoscience applications.[11,19] We found that the 3WJ adopts a nonplanar, Y-shaped structure with unpairing of nucleotides in the vicinity of the branchpoint, producing a nanoscale cavity. Our results provide a structural explanation for the recent demonstration that 3WJs can complex metal helicates[20] and self-assemble into 3D arrays.[21] It is anticipated that the results presented here will guide the development of new dynamic DNA nanostructures and supermolecules.

RESULTS

Distance Restraints from Single-Molecule FRET. The DNA sequence of the 3WJ studied and the positions of the fluorescent dyes are shown in Figure 1a. The sequences are related to those of a forked DNA structure that we recently reported;[17] for the 3WJ, the two 25mer strands of the forked

Received: December 19, 2011
Published: February 13, 2012

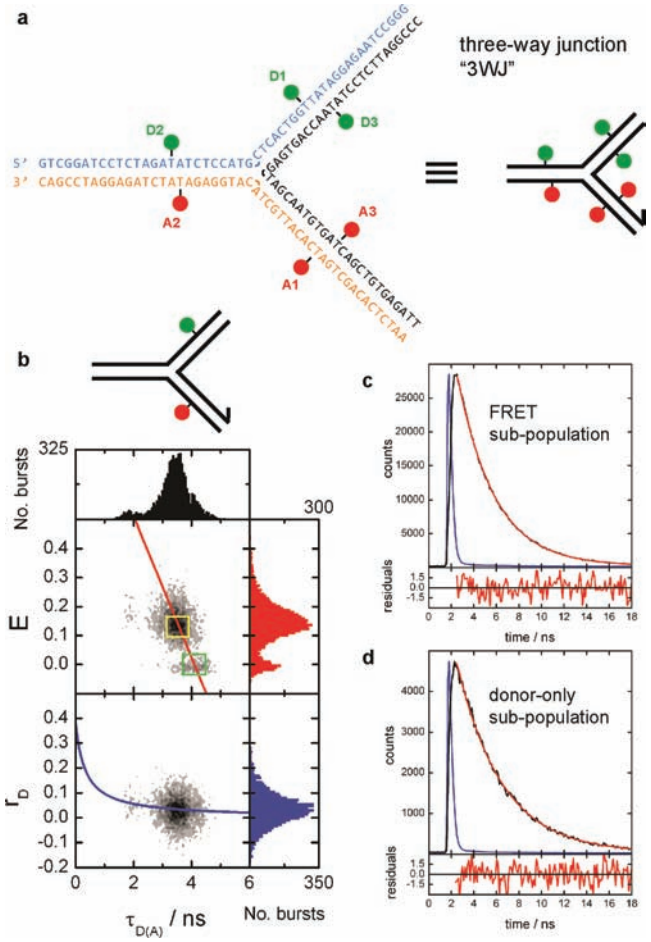

Figure 1. Single-molecule FRET for global structure determination of a 3WJ. (a) DNA sequence and position of donor (D) and acceptor (A) dyes. A simplified representation is depicted on the right. (b) Typical MFD data are shown for a three-way junction labeled with donor and acceptor dyes (positions D1 and A1, see panel a). The 2D plots are of FRET efficiency (E) or donor anisotropy (r_D) versus donor lifetime ($\tau_{D(A)}$). The gray scale indicates an increasing number of single-molecule bursts (from white to black). Also shown are the corresponding 1D histograms. FRET efficiencies were measured from raw green and red signals and corrected for background (1.54 kHz in green; 2.22 kHz in red), spectral crosstalk (3.7%), detection efficiencies (green:red = 0.3), and the fluorescence quantum yields (0.80 for donor; 0.32 for acceptor). The red overlaid line is the theoretical FRET relationship, $E = 1 + \tau_D/\tau_{D(A)}$, with $\tau_D = 4.1$ ns. The blue overlaid line is the Perrin equation, $r_D = r_0(1 + \tau_{D(A)}/\rho_D)$, with mean rotational correlation time $\rho_D = 0.35$ ns and fundamental anisotropy $r_0 = 0.375$. The sample buffer contained 0 mM $MgCl_2$. (c,d) Subensemble time-resolved analysis of the FRET population (from region indicated by yellow box, c) and the donor-only population (from region indicated by green box, d). The decay (black line), instrument response function (blue line), fits to a single-exponential decay reconvoluted with the instrument response (red line), and the corresponding residuals (in red), are shown, with lifetimes of 3.3 ± 0.1 (c) and 4.0 ± 0.1 ns (d); quality of fit or residuals were not improved by fitting to a more complicated decay function.

DNA are joined together. The sequences were designed to form a fully complementary immobile 3WJ via annealing of single strands, with minimal undesirable base pairing (e.g., hairpin formation) or sequence-specific bending. For FRET measurements, each 3WJ sample had a single donor dye, Alexa488, in one of three positions (D1, D2, or D3) and an acceptor dye, Cy5, in one of three positions (A1, A2, or A3). The six dye positions allowed us to measure seven unique distances. We also studied the three donor-only structures, to check for non-FRET effects on the donor fluorescence. In view of the propensity of branched DNA to undergo ion-induced folding,[11] we studied the 3WJ in two buffers, one containing no Mg^{2+} ions and one with 1 mM $MgCl_2$ present.

We employed the technique of multiparameter fluorescence detection (MFD) using a confocal microscope with pulsed laser excitation and four-channel photon-counting detection of fluorescence.[22,23] Figure 1b shows typical SM-FRET data for a donor–acceptor sample (data for each donor–acceptor pair are shown in Figure S1). The 2D plot in Figure 1b is of FRET efficiency (E) or donor anisotropy (r_D) versus donor lifetime ($\tau_{D(A)}$). As discussed previously,[17] MFD allows FRET-related species to be unambiguously assigned, distinct from artifacts due to photobleaching, dye quenching or impurities. The MFD plots are qualitatively the same as those measured for the related forked DNA construct.[17] For donor–acceptor samples, two main populations were observed (Figure 1b); one is identical to that of a donor-only sample (due to unlabeled or photobleached acceptor strand), while the other has a shorter donor lifetime together with reduced donor/acceptor intensity ratio and increased anisotropy. The latter population is due to 3WJ molecules undergoing FRET. As expected for Alexa488 attached to DNA, each donor-only sample has a lifetime of 4.1 ns in all labeling positions. The anisotropy of the donor-only is low, as observed previously, ruling out dye orientation effects.[24]

In order to extract accurate distance measurements, FRET-related structural dynamics must also be considered. Single molecules diffuse through the confocal detection volume in a few milliseconds; dynamics that are faster than this confocal transit time, but slower than the fluorescence decay process, would result in the recording of a nonexponential decay for a single-molecule burst. Use of the FRET efficiency in this case, without further correction, would result in an erroneous distance measurement.[25] For the 3WJ studied here, the FRET species falls on the theoretical "static" FRET line, described by Kalinin et al.[25] This is indicative of a lack of FRET-related dynamics. To investigate this in more detail, we performed a subensemble analysis, by generating the time-resolved decay curve for particular populations.[26]

The results are shown in Figure 1c,d for the FRET and donor populations, respectively. In each case, the subensemble decays can be fitted to a single-exponential decay, with no improvement for the addition of extra decay components or by fitting the FRET subpopulation to a distribution of lifetimes. The residuals show the excellent goodness of fit. Thus, there are no FRET dynamics on the nanosecond to millisecond time scale that would affect the accuracy of the FRET distance measurement, implying that the global structure is relatively static. The precision of our distance experiments, as estimated from repeated measurement, is better than 2 Å. To test the accuracy, we measured SM-FRET distances within two double-stranded DNA (dsDNA) molecules (see Supporting Information and Figure S2). From this, we estimate the accuracy in our measurements to be ca. 2 Å.

Structural Modeling from FRET-Derived Distances. To convert the accurate FRET measurements into absolute dye–dye distances we used a nonlinear conversion function that takes into account the positional and orientational averaging of the dyes. This approach was first reported for dsDNA[24] and used more recently with forked DNA (see Supporting

dx.doi.org/10.1021/ja211802z | J. Am. Chem. Soc. 2012, 134, 6280–6285

Information).[17] The calculated distances for the 3WJ in buffer containing 0 and 1 mM $MgCl_2$ are given in Table 1. These dye−dye distances were used as restraints in molecular dynamics (MD) simulations, as described previously.[17]

Table 1. FRET Distances Calculated from MFD[a]

	DA distance (Å)	
FRET pair	in 0 mM Mg^{2+}	in 1 mM Mg^{2+} [b]
D1A1	69	66
D1A2	64	62
D1A3	68	67
D2A1	71	65
D2A3	81	78
D3A1	69	67
D3A2	66	64

[a]The distances were calculated from the donor lifetime in the presence of acceptor by fitting the lifetime histogram of the FRET subpopulation in MFD plots (e.g., Figure 1b) to a single Gaussian (see Supporting Information). The buffer contained 20 mM Tris and 15 mM NaCl, 1 mM ascorbic acid at pH 7.5. [b]This buffer also contained 1 mM $MgCl_2$. The standard deviation for all distances was within 2 Å.

The helical arms of the 3WJs were modeled and restrained as B-DNA. For the determination of the relative position and orientation of the three arms, six free parameters need to be determined (cf. Figure S6.) with one arm fixed: two polar coordinates and the rotation angle along the long axis for each of the two free arms. The seven unique distances measured are, therefore, sufficient to determine the global structure. For the B-DNA four different sets of restraints were tested: all base pairs restrained (0-free), and one, two, and three base pairs per arm left unrestrained (1-free, 2-free, and 3-free, respectively). The restraints of the bases not only include base pairing but also base stacking. The distance root-mean-square deviation (DRMSD) between the FRET distances and the dye positions in the model measures how well the model fits the measured FRET distances. The DRMSD values for 0 and 1 mM Mg^{2+} buffers are shown in Table S1. The DRMSD is relatively large for the 0-free case, while the 2-free case yields the lowest DRMSD values. The 3-free case did not yield better results in terms of DRMSD, but instead gave less well-defined structures. The 2-free structures with the five lowest DRMSD values were superimposed and are shown in Figure 2a.

Overlays of all 50 structures generated by MD for the 3WJ in the low and high salt buffer are shown in Figure S3, while the effect of different restraints on the structures is illustrated in Figure S4. The structures for 3WJ are well defined, and the global structure is broadly the same regardless of the restraints applied. The structures adopt open Y-shaped conformations, with no apparent coaxial stacking (i.e., base stacking of neighboring helical arms), in contrast to the four-way Holliday junction.[11] The structures are not perfectly symmetrical, and adopt a pyramidal geometry. Small structural differences between the 0 and 1 mM Mg^{2+} samples are evident. In particular, the structures in 1 mM Mg^{2+} are more symmetrical, with similar angles between arms, while the low salt structures deviate more from planarity.

When we studied the related four-stranded fork structure, we saw no evidence for unpairing at the branchpoint, even when two base pairs at the branch were unrestrained.[17] In contrast, the most stable structures here have two base pairs free per arm at the branchpoint. To ensure that minor systematic errors would not cause the observed unpairing, we also carried out MD simulations after applying shifts of ±1 Å to all 7 distances; in fact, the structures were essentially unchanged after applying these shifts (see Figure S5). The unpairing of the bases at the branch allows for the formation of a nanoscale cavity at the branchpoint. As shown in Figure 2b, a cavity with diameter of up to ca. 1.2 nm could be formed, illustrating the potential that such junctions have to act as supramolecular receptors.

Probing Local Branch Structure Using a Nucleobase Analogue. To complement the global structure above, we probed the local DNA structure directly using an alternative fluorescence-based approach. We labeled the same 3WJ sequence used for the FRET studies with 2-aminopurine (2-AP), a fluorescent analogue of adenine (6-AP). It is well known that 2-AP forms stable base pairs with thymine without perturbing the natural structure and behavior of DNA.[27] We

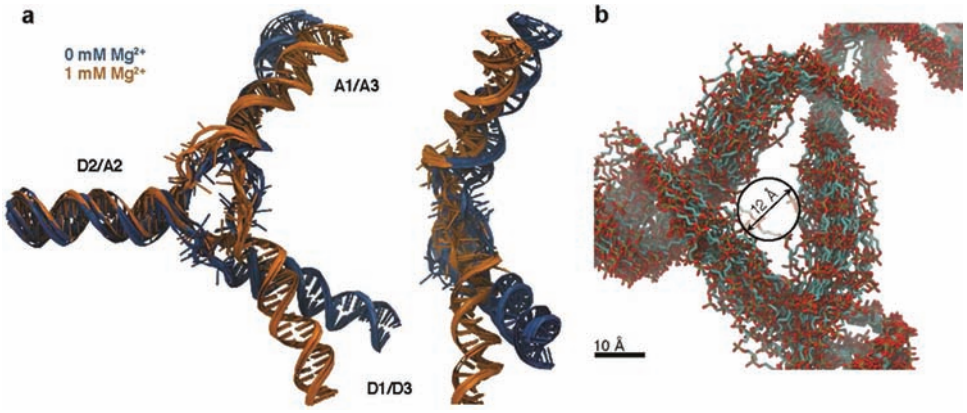

Figure 2. Global structure of 3WJ derived from SM-FRET distance restraints and MD simulations. (a) The five lowest energy structures are shown for 3WJ in buffer containing 0 mM $MgCl_2$ (blue) and 1 mM $MgCl_2$ (orange). The structures are shown from two perspectives, and in each case the structures for the different buffers are overlaid, after aligning the D2/A2 arms. The angles defining the global structure in 0 mM Mg^{2+} are ϕ_1 = (−30.4 ± 14)°, ϕ_2 = (38.7 ± 13)°, θ_1 = (28.5 ± 5.2)°, θ_2 = (72.7 ± 6.2)°; in 1 mM Mg^{2+} they are ϕ_1 = (−26.6 ± 31)°, ϕ_2 = (−61.2 ± 30)°, θ_1 = (65.3 ± 6.8)°, θ_2 = (48.9 ± 5.1)°. The angles are defined relative to arm D2/A2, with subscripts 1 and 2 referring to arms D1/D3 and A1/A3, respectively. See Figure S6 for a geometric model. (b) Close-up view of the branchpoint region for a superposition of the 50 solution structures generated for 3WJ in 0 mM $MgCl_2$. The arrow indicates the diameter of the cavity accessible via unpairing of two basepairs in each arm.

dx.doi.org/10.1021/ja211802z | J. Am. Chem. Soc. 2012, 134, 6280−6285

have shown previously that the time-resolved fluorescence decay profile provides a unique signature of the 2-AP's microenvironment.[18] We studied seven different 3WJ samples, each with a single 2-AP label. The labeling positions are shown in Figure 3a. Since sequence context strongly influences 2-AP

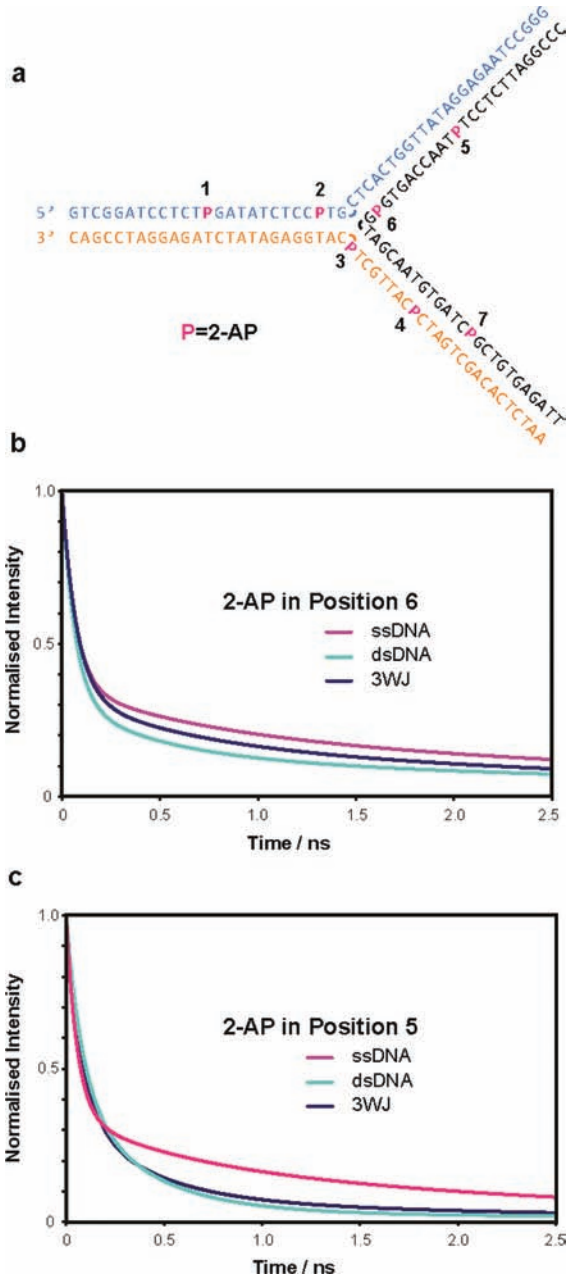

Figure 3. Probing local structure using a fluorescent nucleobase analogue. (a) DNA sequence and position of 2-AP labels. (b,c) Fitted fluorescence decay function for ssDNA, dsDNA, and 3WJ labeled in position 6 (b) and position 5 (c) with 2-AP.

fluorescence, we also studied ssDNA and dsDNA in order to probe the pairing and stacking of 2-AP. We used the same 0 mM Mg^{2+} buffer that was used for SM-FRET. The sequences of the ssDNA and dsDNA samples are given in Supporting Information.

As observed previously, the 2-AP decays are complex and require four decay components to produce a satisfactory fit.[18] The fit parameters are shown in Table S2. The shortest lifetime component of ca. 50 ps corresponds to 2-AP that is well-stacked in the duplex and subject to rapid, interbase fluorescence quenching; the longest component of ca. 10 ns, corresponds to extra-helical 2-AP (free from quenching), while two intermediate lifetimes are attributed to partially stacked forms. The magnitude of the lifetime reveals the nature of microenvironment of the 2-AP (extent of stacking) and the relative weights of the four components indicate the relative populations of the different conformational states. It can be seen that there is significant nearest neighbor stacking in all samples, including ssDNA. Nevertheless, the loss of base pairing (dsDNA cf. ssDNA) is evident in the shift of population from well-stacked to weakly stacked states. The question we ask is whether the 2-AP decay in 3WJs more closely resembles that in ssDNA or dsDNA. We focus here on positions 2−6, which showed large differences in decay profile between ssDNA and dsDNA. In positions 1 and 7, the decays for ssDNA and dsDNA were very similar, precluding their use as probes of pairing.

In Figure 3 we show the fitted decay functions for positions 5 and 6, where the 2-AP is located adjacent to (position 6, Figure 3b) and 12 bases away from (position 5, Figure 3c) the branchpoint. In position 5, the 2-AP decay in the 3WJ looks very similar to that of the duplex control. This supports our assumption that the DNA arms behave like B-DNA. In contrast, the decay for 2-AP in position 6 is intermediate between that of ssDNA and dsDNA, indicating significant unpairing.

Overall, our time-resolved data suggests that significant perturbation of the 3WJ only occurs at the branch (e.g., position 3) and one base away from the branch (e.g., position 6). The decays for 2-AP in all other positions look similar to those of duplex DNA. We found that plotting the product of the pre-exponential "A-factor" and the lifetime for each component provides a good empirical indicator of unpairing. These plots for positions 2−6 are shown in Figures S7 and S8. It should be noted that the decays for 2-AP far from the branchpoint do not correspond exactly to those of the respective duplex controls, suggesting that the perturbation at the branch exerts a structural influence up to a helical turn away from the branch.

■ DISCUSSION

Little is known of the structures of three-way DNA junctions as compared with four-way DNA Holliday junctions.[11] The 3WJ DNA junction is potentially formed *in vivo* during unfolding, recombination and repair when ssDNA is present,[28] while RNA 3WJs have been more widely studied, and are prevalent in nature both in naked RNA and in ribonucleoprotein complexes.[11] In addition, DNA and RNA 3WJs are critical components in many nanoscience applications.[19,29] The majority of reports of DNA and RNA three-way junctions have focused on bulged 3WJs, where additional nucleotides are inserted at the branchpoint rather than the fully complementary, so-called "perfect", 3WJ analyzed here and prevalent both in nature and in nanoassemblies. Earlier ensemble experiments were inconclusive as to the nature of the global structure of 3WJ.[30−34] In contrast, we are able to show that the 3WJ reported here adopts a well-defined Y-shaped structure with pyramidal geometry, regardless of the presence or absence of $MgCl_2$, although $MgCl_2$ does have some impact on junction structure. With bulged three-way junctions and four-way DNA junctions, magnesium ion-induced conformational changes

dx.doi.org/10.1021/ja211802z | J. Am. Chem. Soc. 2012, 134, 6280−6285

usually occur below 1 mM Mg^{2+}.[11,32] However, the presence of 1 mM $MgCl_2$ has a relatively minor effect here, as anticipated from previous studies,[11] and we do not observe the coaxial stacking that is seen in four-way junctions.[11] The similarity of 2-AP fluorescence decays in 3WJ and dsDNA for positions 2, 4, and 5 validates our assumption that the 3WJ arms behave like duplex DNA. The minor differences observed in these positions may indicate that a small structural perturbation extends beyond the branch region, as suggested previously.[30]

Unexpectedly, our FRET-based global structure determination also indicated the unpairing of base pairs near the branchpoint. A number of studies have previously probed the dynamics and local branch structure of 3WJs. DNA cyclization experiments suggested that the 3WJ is a very flexible structure.[35] The branches of 3WJs were postulated to have variable angles of 60−90° between arms, indicative of flexibility.[33] Enzyme cleavage experiments also suggested a flexible structure.[28] It was proposed that there might be local unfolding/plasticity in the branchpoint structure, in which at least one basepair at the branch breaks transiently,[19] consistent with chemical footprinting experiments using single strand-specific reagents.[30,33] Breakage of base pairs at or near the branch point would also explain why flanking bases govern the conformation, as suggested by earlier comparative gel electrophoresis experiments.[36,37] Our FRET-based model and the 2-AP studies imply that branch flexibility may be an inherent feature of 3WJs as a result of local unpairing at the branchpoint.

CONCLUSIONS

In summary, we have applied quantitative SM-FRET and MD simulations to determine the global structure of an important branched DNA in solution with high accuracy, and free from interference from surfaces or sample heterogeneity. The observation of unpaired bases in fully complementary junctions is likely to have implications for understanding the way in which branched DNA interacts with proteins *in vivo*. Our findings are also of direct relevance to the growing field of DNA and RNA nanoscience. Much of the spectacular success of DNA and RNA nanoscience has been based upon hydrogen-bond complementarity to produce stable structures. Although 3WJs were prominent components of early DNA nanoscience research, their use as nanostructural components was limited, primarily because of the flexibility discussed above.[38] However, a number of recent reports have described perfect DNA 3WJs bound to metal complexes to produce stable supramolecular species[20] and self-assembled arrays.[21] RNA 3WJs have also been used as a core motif in the formation of functional nanoparticles for therapeutic applications.[29] There is also a move toward developing dynamic nucleic acid structures. This has focused primarily on kinetically controlled strand displacement,[39] but the branch flexibility described here could be utilized in alternative forms of dynamic self-assembly (e.g., via complexation at the branchpoint). Furthermore, it has recently been demonstrated that helical stacking between nanostructures can be used to control self-assembly.[40] Here, we have shown that unpairing, presumably due to steric strain and local stacking interactions rather than hydrogen bonding, can predominate. In both cases, Watson−Crick complementarity is not the only important factor in determining the most stable structure. Indeed, the importance of base-stacking contributions to DNA stability is now widely accepted.[41] This work opens up new possibilities for the design of nucleic acid nanosystems and aids in the understanding of molecular recognition involving DNA-based supermolecules.

MATERIALS AND METHODS

Preparation of Branched DNA. Oligonucleotides were synthesized and labeled (Purimex GmbH, Grebenstein) using NHS-esters of Alexa488 (5′/6′ mixed isomer, Invitrogen) or Cy5 (GE-Healthcare), or 2-AP phosphoramidite (Glen Research). Annealing of samples for branched DNA was carried out in buffer (13 mM Tris, 65 mM NaCl, pH 7.5). Annealing buffer for duplexes contained 16 mM Tris and 80 mM NaCl. For all structures, the ratio of donor strand to other strands was 1:3. Samples were heated to 90 °C in a water bath and left to cool slowly overnight. For measurement, all samples were diluted into buffer containing 20 mM Tris, 15 mM NaCl, and 1 mM ascorbic acid at pH 7.5. Prior to sample addition, buffer was stirred with activated charcoal to remove fluorescent impurities. The buffer for high salt experiments also contained 1 mM $MgCl_2$.

Single-Molecule Fluorescence Spectroscopy. For single-molecule measurements in solution, we used a home-built MFD setup, which is based around a confocal microscope with photon-counting detection (Becker and Hickl) and pulsed laser excitation (Picoquant), allowing the simultaneous measurement of fluorescence intensity, color, lifetime, and polarization (see Supporting Information for full details of the MFD setup). All measurements were recorded at 21 ± 1 °C. Data analysis for MFD used software written by the group of Prof. Claus Seidel (Heinrich Heine Universität, Düsseldorf). Subensemble analyses used DAS6 software from HORIBA Jobin Yvon.

Molecular Modeling. The program CNS[42] was used for the simulated annealing molecular dynamics calculation, as described previously.[17] In brief, FRET distance restraints were applied to model the geometry of the DNA. We used the mean dye positions for Alexa488 and Cy5 obtained from a MD simulation that has been published previously.[24] Those mean positions were then fixed relative to the surface of the DNA by distance restraints. The distance restraints were generated by the DEN (Deformable Elastic Network) feature[43] in CNS which selects random atom pairs that are within a specified distance range in the starting structure. The starting temperature for the simulated annealing was 3000 K and decreased to 0 K within 15 ps. Full details are given in the Supporting Information .

Time-Resolved Ensemble Fluorescence Spectroscopy. Time-resolved fluorescence spectroscopy was performed using the technique of time-correlated single photon counting, using an Edinburgh Instruments spectrometer equipped with TCC900 photon counting electronics. The excitation source was the third harmonic of a pulse-picked Ti-Sapphire femtosecond laser system (Coherent, 10 W Verdi, and Mira Ti-Sapphire) producing pulses of ca. 200 fs at a repetition rate of 4.75 MHz. The instrument response function (IRF) was ca. 70 ps full width at half-maximum. Decay curves were analyzed using a standard iterative reconvolution method, assuming a multiexponential decay function. Fluorescence was excited at 310 nm, and decay curves were recorded at three emission wavelengths, 370, 380, and 390 nm. The three decays were analyzed globally using Edinburgh Instruments "FAST" software. The quality of fit was judged on the basis of the reduced chi-square statistic, χ^2, and the randomness of residuals. See Supporting Information for further details.

ASSOCIATED CONTENT

Supporting Information

Sample preparation; experimental and computational methods. This material is available free of charge via the Internet at http://pubs.acs.org.

AUTHOR INFORMATION

Corresponding Author

steven.magennis@manchester.ac.uk; gu.schroeder@fz-juelich.de

Notes

The authors declare no competing financial interest.

■ ACKNOWLEDGMENTS

We thank the BBSRC for support (BB/G00269X/1); Claus Seidel, Ralf Kühnemuth, and Stefan Marawske for assistance in developing our MFD setup; Suren Felekyan for help with data analysis; and Jochen Arlt for assistance with experiments. S.W.M. acknowledges the award of an EPSRC advanced research fellowship (EP/D073154), and L.M. acknowledges the award of a CSC scholarship.

■ REFERENCES

(1) Atkinson, J.; McGlynn, P. *Nucleic Acids Res.* **2009**, *37*, 3475−3492.
(2) Heller, R. C.; Marians, K. J. *Nat. Rev. Mol. Cell Biol.* **2006**, *7*, 932−943.
(3) Seeman, N. C. *Nano Lett.* **2010**, *10*, 1971−1978.
(4) Aldaye, F. A.; Palmer, A. L.; Sleiman, H. F. *Science* **2008**, *321*, 1795−1799.
(5) Guo, P. X. *Nature Nanotechnol.* **2010**, *5*, 833−842.
(6) Lund, K.; Manzo, A. J.; Dabby, N.; Michelotti, N.; Johnson-Buck, A.; Nangreave, J.; Taylor, S.; Pei, R. J.; Stojanovic, M. N.; Walter, N. G.; Winfree, E.; Yan, H. *Nature* **2010**, *465*, 206−210.
(7) Gu, H. Z.; Chao, J.; Xiao, S. J.; Seeman, N. C. *Nature* **2010**, *465*, 202−205.
(8) Zheng, J. P.; Birktoft, J. J.; Chen, Y.; Wang, T.; Sha, R. J.; Constantinou, P. E.; Ginell, S. L.; Mao, C. D.; Seeman, N. C. *Nature* **2009**, *461*, 74−77.
(9) Yin, P.; Choi, H. M. T.; Calvert, C. R.; Pierce, N. A. *Nature* **2008**, *451*, 318−322.
(10) Rothemund, P. W. K. *Nature* **2006**, *440*, 297−302.
(11) Lilley, D. M. J. *Q. Rev. Biophys.* **2000**, *33*, 109−159.
(12) Sisamakis, E.; Valeri, A.; Kalinin, S.; Rothwell, P. J.; Seidel, C. A. M. *Methods Enzymol.* **2010**, *475*, 455−514.
(13) Brunger, A. T.; Strop, P.; Vrljic, M.; Chu, S.; Weninger, K. R. *J. Struct. Biol.* **2011**, *173*, 497−505.
(14) Weiss, S. *Science* **1999**, *283*, 1676−1683.
(15) Roy, R.; Hohng, S.; Ha, T. *Nat. Methods* **2008**, *5*, 507−516.
(16) McKinney, S. A.; Déclais, A. C.; Lilley, D. M. J.; Ha, T. *Nat. Struct. Biol.* **2003**, *10*, 93−97.
(17) Sabir, T.; Schröder, G. F.; Toulmin, A.; McGlynn, P.; Magennis, S. W. *J. Am. Chem. Soc.* **2011**, *133*, 1188−1191.
(18) Neely, R. K.; Daujotyte, D.; Grazulis, S.; Magennis, S. W.; Dryden, D. T. F.; Klimasauskas, S.; Jones, A. C. *Nucleic Acids Res.* **2005**, *33*, 6953−6960.
(19) Seeman, N. C.; Kallenbach, N. R. *Annu. Rev. Biophys. Biomol. Struct.* **1994**, *23*, 53−86.
(20) Oleksi, A.; Blanco, A. G.; Boer, R.; Usón, I.; Aymamí, J.; Rodger, A.; Hannon, M. J.; Coll, M. *Angew. Chem., Int. Ed.* **2006**, *45*, 1227−1231.
(21) Boer, D. R.; Kerckhoffs, J.; Parajo, Y.; Pascu, M.; Usón, I.; Lincoln, P.; Hannon, M. J.; Coll, M. *Angew. Chem., Int. Ed.* **2010**, *49*, 2336−2339.
(22) Rothwell, P. J.; Berger, S.; Kensch, O.; Felekyan, S.; Antonik, M.; Wohrl, B. M.; Restle, T.; Goody, R. S.; Seidel, C. A. M. *Proc. Natl. Acad. Sci. U.S.A.* **2003**, *100*, 1655−1660.
(23) Gansen, A.; Valeri, A.; Hauger, F.; Felekyan, S.; Kalinin, S.; Tóth, K.; Langowski, J.; Seidel, C. A. M. *Proc. Natl. Acad. Sci. U.S.A.* **2009**, *106*, 15308−15313.
(24) Woźniak, A. K.; Schröder, G. F.; Grubmüller, H.; Seidel, C. A. M.; Oesterhelt, F. *Proc. Natl. Acad. Sci. U.S.A.* **2008**, *105*, 18337−18342.
(25) Kalinin, S.; Valeri, A.; Antonik, M.; Felekyan, S.; Seidel, C. A. M. *J. Phys. Chem. B* **2010**, *114*, 7983−7995.
(26) Laurence, T. A.; Kong, X. X.; Jäger, M.; Weiss, S. *Proc. Natl. Acad. Sci. U.S.A.* **2005**, *102*, 17348−17353.
(27) Wilhelmsson, L. M. *Q. Rev. Biophys.* **2010**, *43*, 159−183.
(28) Jensch, F.; Kemper, B. *EMBO J.* **1986**, *5*, 181−189.
(29) Shu, D.; Shu, Y.; Haque, F.; Abdelmawla, S.; Guo, P. X. *Nature Nanotech.* **2011**, *6*, 658−667.
(30) Duckett, D. R.; Lilley, D. M. J. *EMBO J.* **1990**, *9*, 1659−1664.
(31) Stühmeier, F.; Welch, J. B.; Murchie, A. I. H.; Lilley, D. M. J.; Clegg, R. M. *Biochemistry* **1997**, *36*, 13530−13538.
(32) Welch, J. B.; Duckett, D. R.; Lilley, D. M. J. *Nucleic Acids Res.* **1993**, *21*, 4548−4555.
(33) Shlyakhtenko, L. S.; Rekesh, D.; Lindsay, S. M.; Kutyavin, I.; Appella, E.; Harrington, R. E.; Lyubchenko, Y. L. *J. Biomol. Struct. Dyn.* **1994**, *11*, 1175−1189.
(34) Shlyakhtenko, L. S.; Potaman, V. N.; Sinden, R. R.; Gall, A. A.; Lyubchenko, Y. L. *Nucleic Acids Res.* **2000**, *28*, 3472−3477.
(35) Ma, R. I.; Kallenbach, N. R.; Sheardy, R. D.; Petrillo, M. L.; Seeman, N. C. *Nucleic Acids Res.* **1986**, *14*, 9745−9753.
(36) Lu, M.; Guo, Q.; Kallenbach, N. R. *Biochemistry* **1991**, *30*, 5815−5820.
(37) Zhong, M.; Kallenbach, N. R. *J. Mol. Biol.* **1993**, *230*, 766−778.
(38) Seeman, N. C.; Lukeman, P. S. *Rep. Prog. Phys.* **2005**, *68*, 237−270.
(39) Zhang, D. Y.; Seelig, G. *Nature Chem.* **2011**, *3*, 103−113.
(40) Woo, S.; Rothemund, P. W. K. *Nature Chem.* **2011**, *3*, 620−627.
(41) Yakovchuk, P.; Protozanova, E.; Frank-Kamenetskii, M. D. *Nucleic Acids Res.* **2006**, *34*, 564−574.
(42) Brunger, A. T. *Nat. Protoc.* **2007**, *2*, 2728−2733.
(43) Schröder, G. F.; Brunger, A. T.; Levitt, M. *Structure* **2007**, *15*, 1630−1641.